JOINT EUROPEAN TORUS

JET–P(92)97

G.J. Kramer, A.C.C. Sips, N.J. Lopes Cardozo
and JET Team

Electron Density Fluctuation in JET Measured with Multichannel Reflectometry

Electron Density Fluctuation in JET Measured with Multichannel Reflectometry

G.J. Kramer[1], A.C.C. Sips, N.J. Lopes Cardozo[2]
and JET Team*

JET-Joint Undertaking, Culham Science Centre, OX14 3DB, Abingdon, UK

[1]On attachment from FOM Rijnhuizen, Nieuwegein, The Netherlands.
[2]FOM Rijnhuizen, Nieuwegein, The Netherlands
** See Annex*

Preprint of Paper to be submitted for publication in
Plasma Physics and Controlled Fusion

Electron density fluctuation in JET measured with multichannel reflectometery.

G.J. Kramer*, A.C.C. Sips and N.J. Lopes Cardozo**.

JET joint undertaking, Abingdon, Oxon, OX14 3EA.

*) On attachment from FOM Rijnhuizen, Nieuwegein, The Netherlands.

**) FOM Rijnhuizen, Nieuwegein, The Netherlands.

Abstract

Electron density fluctuations have been studied with the multichannel refelectometer at JET. Results from three topics are presented: the location of MHD modes, fluctuations during the sawtooth crash and fluctuations before and after the L-mode to H-mode transition. The non-linear response of the homodyne detection system, used to measure density fluctuations is considered. This can introduce artefacts in the data which should be taken into account in the interpretation of the signals.

1. Introduction

In the search for possible physical mechanisms that could account for for the anomalous transport in tokamak plasmas, many experiments have been performed to measure fluctuations or micro turbulence in the plasma [see e.g Liew85 and references therein]. Often fluctuations of the electron density have been studied as a manifestation of micro turbulence. These have been measured amongst others with langmuir probes [RhoR90], Heavy-ion-beam probes [SchC88] and various light scattering experiments [BroP87]. Recently, microwave reflectometry has also become available to study density fluctuations. An overview on the present status of microwave reflectometry as a diagnostic tool for fusion plasmas can be found in ref. [IAEA92]. Reflectometry is not restricted to the plasma edge as in the case of langmuir probes and its scattering plane is well localized in the plasma. The drawback, however, is that it is unselective in the range of k-vectors of the plasma turbulence [HolR92b].

In the basic set-up of a reflectometer, a microwave beam is launched into the plasma and reflected off the density layer beyond which the waves cannot propagate. The reflected waves can be detected with either a homodyne or a heterodyne system. A homo-

dyne detection system is more easy to build than a heterodyne detector, but as we will discuss in this paper the interpretation of the signals is very difficult due to non-linear responses to plasma movement and fluctuations. Attempts have been made to calculate the detector response to density fluctuations from simple one-dimensional [Crip92,Hutc92] and two-dimensional models [HolR92a] but to date the agreement between theory and experiment is not satisfactory.

The multichannel reflectometer at JET [HugP86,PreC86] which we have used for the present study is fitted with both detection systems. The heterodyne detectors are used to monitor the (slow) profile evolution [SipK92] whereas the homodyne detectors are used for fluctuation measurements. As a result, we can follow the movements of the electron density profiles as well as the evolution of the amplitude of broadband fluctuations frequency as a function of time and space.

Reflectometry measurements have already been used for a number of studies i.e. for edge density profile measurements [SipK92], and during (rapidly) changing plasma conditions such as sawteeth [HogR91], ELM's [ColC92] and MHD activity [KraS92]. Recently, radial correlation lengths in the plasma were obtained as well by using correlation techniques between signals coming from two different positions in the plasma [Crip92]. In principle this technique could also be applied to different channels of the multichannel reflectometer system. However, using the homodyne signals for such a study results in an underestimate of the coherence between channels due to the highly non-linear behaviour of the homodyne detectors. Therefore, in this paper we will not pursue correlation techniques.

In this paper we first give an introduction to the basic set-up of the JET multichannel reflectometer (Sec. 2), followed by a discussion of the signals arising from the homodyne detection system with its non-linearities (Sec. 3). In Sec. 4 we discuss the relation between measured signals and the fluctuations in the plasma. In spite of the difficulties arising from the non-linear behaviour of the detection system we have been able to obtain experimental results. These are presented in Sec. 5. The topics which we study there are i) the localization of MHD modes, ii) the behaviour of high frequency density fluctuations during sawteeth and iii) the change in fluctuations from the L-mode to H-mode state of the plasma. Finally, in Sec. 6 conclusions are drawn.

2. Instrumentation

The JET multichannel reflectometer consists of twelve channels which probe densities between 0.4 and 8.0 10^{19} electrons/m^3. The system operates in O-mode i.e. the lectric field of the wave is launched parallel to magnetic field in the torus. In this configuration the propagation of the wave and its reflection point in the plasma are independent of the magnetic field. The microwaves, with angular frequency ω, are reflected at a critical density layer, n_e, which is given by $\omega = \omega_{pe}$, the electron plasma frequency. In table 1 the frequencies used in the JET reflectometer are given together with their critical densities. In Fig. 1 the basic layout for one single channel is given. Each channel consists of a tuned transmitter and receiver Gunn diode pair. For each channel a small fraction of the microwave power is transmitted through a reference arm. The rest of the power is combined with that of the other channels in one oversized waveguide, transported to the torus and launched into the plasma. Separate antennae and waveguides are used for the launching and receiving systems in order to avoid spurious reflections. At the detectors the signals are down-converted to 10.7 MHz, the IF frequency of the receivers. The plasma signal has undergone a phase shift compared to the 10.7 MHz IF from the reference arm. From this phase shift the (slow) evolution of the critical density layers is obtained with an accuracy of less than 0.5 cm [SipK92] and from the phase change during a narrow band sweep, absolute positions of the reflection layers in the plasma can be obtained with an uncertainty of less than 3 cm [Sips91]. The phase detectors, however, are restricted in their frequency response to 3 kHz in order to suppress spourious signals (the so called phase runaway) due to "phase noise" created by density fluctuations in the plasma. A full description of the detection system of the reflectometer can be found in [Huge90].

3. The homodyne detection system

In order to study broadband electron density fluctuations at the same time as measuring the evolution of the electron density profile, the reflectometer is also equipped with homodyne detectors. These detectors use the same 10.7 MHz IF signal, so we are able to measure simultaneously the positions and the fluctuations of the critical density layers. The fluctuation spectra presented in this paper are measured with a low-pass detection bandwidth of 100 kHz. Homodyne detectors are sensitive to both amplitude

and phase fluctuations:

$$V(t) = A(t)\cos(\phi(t)), \tag{1}$$

where $V(t)$ is the detector output, $A(t)$ the amplitude of the signal and $\phi(t)$ the phase difference between the signals from the plasma arm and the reference arm.

In order to investigate the phase response of the homodyne detection system we assume a constant amplitude signal, A_0, and a reflection layer at an equilibrium distance, giving rise to a fixed phase angle, ϕ_0. To the equilibrium position of the layer we add a spectrum of (small) random movements, $\phi(\omega, t)$. After making a Taylor expansion of the cosine function around ϕ_0 and after taking the Fourier transform (with $\phi(\omega, t) = f(\omega)\exp(i\omega t)$) we obtain:

$$V(\omega) = \frac{A_0}{\sqrt{2\pi}}[\cos(\phi_0) - \sin(\phi_0)f(\omega) - \frac{\cos(\phi_0)}{2}f(\omega)^2 + ...]. \tag{2}$$

This equation immediately shows that i) the initial phase ϕ_0 dominates the response of the detector, ii) higher "ghost" harmonics are generated in the output and iii) under unfavourable conditions ($\phi_0 = \pm n\pi$) the frequency, ω, disappears completely from the output signal. Graphically, these effects are shown in Fig. 2. At the zero crossing of $\cos(\phi_0)$ small phase fluctuations show up linearly in the output whereas at the top of $\cos(\phi_0)$ the frequency doubles and the output amplitude is reduced compared to the linear response part.

Experimentally these effects are observed as shown in Fig. 3. In this example a strong MHD mode was present at 3.2 kHz, but we observe this mode also at its higher harmonics. The equilibrium distance of the critical density layer was slowly moving; so ϕ_0 is also varying (see Fig. 4b). Each time when $\cos(\phi_0)$ passes through zero we observe a maximum amplitude in the fundamental frequency (see Fig. 4c) whereas the second harmonic has its minimum. Conversely, when $\cos(\phi_0)$ passes through a maximum or a minimum the fundamental frequency is almost, but not completely, suppressed, while the second harmonic reaches its maximum (see Fig. 4d). In the spectrum (Fig. 3) the third and fourth harmonic are also observable. They are also ruled by the behaviour of the detector response of the slow movement of the reflection layer as can be seen from Figs. 4e and 4f.

From Eq. 2 it is expected that the fundamental frequency is completely suppressed at the maxima and minima of the slow signal. In the analysis which leads to Eq. 2 we have omitted amplitude fluctuations. When the phase modulation vanishes due to an

unfavourable initial phase, ϕ_0, the amplitude modulation becomes visible as can be seen from the non-vanishing signal at the minima in the fundamental frequency (see Fig. 4c). However, the system is less sensitive to amplitude modulation, hence the rather small residual response.

4. Physics interpretation

From the discussion of the non-linear behaviour of the homodyne detector system it is clear that its signals are difficult to interpret. In this section we address the question of the physical interpretation of these signals.

First of all, it should be noted that a fluctuation measurement with a reflectometer is in principle a non-local measurement; the probing microwave beam is influenced by the (lower density) plasma layers between the antenna and the reflection layer. Experimentally, however, it is found that the microwave beams are only affected by the density fluctuations very close to, and at, the critical density layer. This is concluded from the observations of MHD modes which are localized at the edge. These modes show only up in one or two edge channels whereas signals from channels (one or two centimeters) more inside do not measure of these modes. Such a case will be shown in Fig. 8 of Sec. 5.1 where the 15 kHz mode is confined to the edge and not observed on channels reflecting from layers further inside the plasma.

The range of k-vectors which are accessed by the reflectometer depends on the relative position between the transmittor and receiver antennas. At JET the antennas are placed at the same toroidal position, close to the midplane. Thus, in the poloidal and toroidal direction small k-vectors are accessed whereas in the radial direction this range is large due to the possible backscattering of the microwaves in front of the reflecting layer.

A further complication of the reflectometer system is that it it consists of twelve independent channels with different microwave powers and attenuations. Therefore it is very difficult to obtain a reliable relative calibration of the fluctuation levels between the different channels. A further complication is presented by the non-linear response of the homodyne detectors to phase fluctuations. Often, we observe discrete MHD modes on different channels of the reflectometer (see Figs. 5 and 9). In order to be able to compare relative sizes of these discrete modes in different channels we normalize the discrete mode to the local continuous background for each channel separately and compare these

numbers. The amplitude of the broadband background of density fluctuations is a slowly varying continuous function of the plasma minor radius coordinate, wheraes the discrete modes are confined to small regions inside the plasma. From these non-dimensional numbers for different channels, which give the increase of the density fluctuations due to the MHD mode, we can determine the radial extent of the MHD mode. This normalisation is only valid when the phase fluctuations caused by the MHD mode are less than π.

It is not possible to deduce radial displacements of the fluctuations around the equilibrium positions of the probed density layers from the homodyne detector signals due to the mentioned mixture of phase and amplitude fluctuations. However, if we observe a fundamental frequency signal without (strong) higher harmonics we can estimate an upper limit for these displacements under the assumption that the signal is dominated by the phase fluctuations. Then the upper limit of the layer movement, $\tilde{x}_u$, is given by:

$$\tilde{x}_u = 0.25\lambda_0 \tag{3}$$

where λ_0 is the vacuum wave length of the probing microwave. The factor 0.25 takes into account that both the initial and reflected wave paths are affected by the movement (factor 0.5) and from the assumption that we do not observe higher harmonics i.e. phase fluctuations are restricted to less than π (factor 0.5, see Fig. 2). The maximum wavelength which we use in the reflectometer is 1.6 cm, so under the above given conditions the upper limit of $\tilde{x}_u$ is less than 0.4 cm.

Since we are probing layers of constant density, we observe radial displacement fluctuations, $\tilde{x}$, of these layers. The displacements can be transformed to density fluctuations, $\tilde{n}$, if the local density gradients are known:

$$\tilde{n} = \frac{\partial n}{\partial x}|_{n_e}\tilde{x}. \tag{4}$$

The density profile can be obtained from phase measurements by the heterodyne detection system of the JET reflectometer. A full report on the profile reconstruction technique for the JET multichannel reflectometer is given in ref. [SipK92].

A very important question for the interpretation of fluctuations measured with the reflectometer is whether the principal source is local density fluctuations or deformations of the reflecting surface. The former is typical for electrostatic turbulence where the fluctuations arise as a result of drift motions of the plasma across the fiield lines. In the

second case magnetic modes are responsible for a rippling of the flux surface. In general we cannot distinguish between these two sources of the density fluctuations. However, for discrete modes which are observed simultaneously with pick-up coils, we can certainly say that those fluctuations are induced magnetically, i.e. by ripples on magnetic flux surfaces. The signature of the broadband background is much more difficult to access. Comparison with signals from magnetic pick-up coils is not possible because the pick-up coils are neither sensitive to magnetic signals arising from high mode numbers nor to electrostatic fluctuations.

5. Topical studies

In this section we present density fluctuation measurements obtained with the JET multichannel reflectometer for selected plasma conditions. In Sec. 5.1 we will focus the attention to the discrete MHD modes in order to obtain information on the localization of these modes. In Sec. 5.2 we investigate the behaviour of high frequency density fluctuations during and after the sawtooth crash. In Sec. 5.3 we investigate the behaviour of the density fluctuations before and after the L-mode to H-mode transition. During this transition a transport barrier is formed at the plasma edge. We investigate to what extent the density fluctuations are modified at this transition. A overview of the plasma conditions of the pulses we have used for these studies is given in table 2.

5.1 Localisation of MHD activity

In Fig. 5 we show a density fluctuation spectrum for the channel which is reflecting off a critical density $n_e = 3.14\ 10^{19}\ m^{-3}$. On top of a broadband background of density fluctuations a number of discrete modes are observed together with one very strong mode at 1.8 kHz. In the same figure we show a spectrum taken with a magnetic pick-up coil at the same time as the density spectrum. Here too, the 1.8 kHz mode is the dominant feature. The time traces for the reflectometer and pick-up coil signals are shown in the upper and lower part of Fig. 6, respectively. From the magnetic trace it is clear that the 1.8 kHz signal can be identified as a so called fishbone instability. In the reflectometer signal this is not immediately clear but if we apply a bandpass filter from 1 kHz to 5 kHz then the correlation between the magnetic and reflectometer signals is striking (see Fig. 6).

For the first few milliseconds, especially between 4 and 7 milliseconds, the reflectometer signal is severely distorted due to the non-linear behaviour of the homodyne detection system which was discussed before. At the time of the onset of the fishbone the reflection layer is in such a position that the fundamental frequency of the phase fluctuations are suppressed completely. However, from this suppression we can conclude that the oscillations detected later are generated by phase fluctuations and not by amplitude fluctuations. The radial extent as determined by the technique described in Sec. 4, is shown in Fig. 7 together with the q-profile. In so far as the limited number of channels allows, we see that the fishbone peaks around the q=1 surface and vanishes towards the edge (at 4.18 m).

In a similar discharge, two other MHD modes were exited. Their radial extents are shown in Fig. 8. The 1.5 kHz mode seems to coincide with the q=2.5 surface whereas the 15.7 kHz mode is located at the edge.

The third example of MHD activity as seen by the reflectometer is a high-β, H-mode discharge. The density fluctuation spectrum is shown in Fig. 9 where it can be seen that the broadband part of the spectrum is rather flat up to 100 kHz and does not show the fall off at the high frequencies as the L-mode spectrum (Figs. 3 and 5). We can even observe a broad structure between 30 and 100 kHz. Here we want to concentrate on two MHD modes, the one at 2.4 kHz and the one at 20 kHz. These modes are also visible on the magnetic signal which is also shown in Fig. 9. The evolution of the spectrum shows that the 2.4 kHz mode is only present in the 20 ms before the onset of the mode at 20 kHz.

From the time trace of the magnetic signal (not shown here) it is clear that the 20 kHz mode is again a fishbone. We observe the mode in the five channels outside the q=1 surface, especially in the two channels at the edge (see Fig. 10). Our measurements indicate an increase of the mode towards the q=1 surface as well (Fig. 10) but a better radial coverage of the reflectometer channels is needed to confirm this observation. From soft x-rays signals a similar behaviour was found by Nave et al. [NavC90]. They observed the fishbone activity in high-β pulses through the whole plasma with two maxima, located at the q=1 surface and at the edge.

At this stage we might question the validity of the normalization for the edge channels. As it will be shown shortly that the level of radial displacement fluctuations, $\tilde{x}$, at the edge drops significantly in the H-mode compared to the L-mode (see Fig. 13), it

can thus be argued that the normalization of the MHD modes to the background fails. However, if we determine the localization of the 2.4 kHz mode, which is present in te plasma 20 ms before the onset of the fishbone, we see that it peaks at 4.02 m, at the q=3 surface and drops again towards the edge. From this it is concluded that the 20 kHz mode does indeed have a strong component at the edge.

Measurements of the toroidal plasma rotation yield a frequency of 20 kHz in the centre of the plasma, which is in agreement with the observed frequency for n=1 modes. An estimate of the toroidal rotation at 4 m gives a frequency of 2.5 kHz which agrees well with the observed frequency of the 2.4 kHz mode before the onset of the fishbone. It is noted that the 20 ms before the onset of fishbone the mode at 2.4 kHz may have the local fluid velocity. Mode coupling, which is often involved if different modes are observed at the same frequency, can not occur because the fishbone is not yet present. It is possible that the edge mode persists during the fishbone but is speeded up to 20 kHz through mode couping. However, the amplitude and localization of the edge fluctuations undergo a marked change when the fishbone comes up, indicating that there is a significant direct contribution of the fishbone instability to the edge fluctuations.

5.2 Fluctuations during heat pulse propagation

It is well known that the electron heat diffusivity deduced from sawtooth heat pulse propagation (χ^{hp}) is usually significantly larger than the value obtained from power balance analysis (χ^{pb}). In [TubL87] the difference is attributed to the fact that heat pulse propagation yields a measurement of $\chi^{inc} = \partial q_e/\partial \nabla \mathrm{T}$, while power balance analysis evaluates $\chi^{eff} = q_e/\nabla \mathrm{T}$ (q_e denotes the electron heat flux). The difference arises if χ^{eff} has a $\nabla \mathrm{T}$ dependence. In this case χ^{eff} undergoes a modest increase during the passage of the heat pulse, in concurrence with the increase of the temperature gradient. Depending on the amplitude of the heat pulse, the increase of χ^{eff} is typically up to about 10%. It might be expected that to this increase an increase of the fluctuation level is correlated. This needs only be in the order of 5%, which is not measurable with the present accuracy. Alternatively, it has been proposed that the rapid propagation of the heat pulse is caused by a considerable enhancement due to strong turbulence excited by the sawtooth crash itself [FreM90]. In this model, a strong increase of the turbulence level in the sawtooth propagation region is expected during about 1 ms after

the crash. Measurements of density fluctuations might be used to distinguish between these models.

In the past, electron density fluctuations have been measured during the sawtooth crash by Brower et al. [BroP87] in the TEXT tokamak, using a far infrared laser scattering (FIR) diagnostic. They observed an increase of the density fluctuation level at the fast collapse phase of the sawtooth crash. Their system was focused close to the center of the plasma, inside the mixing radius. No information was obtained for the density fluctuations outside the mixing radius where the heat pulse is propagating. In a second experiment, performed by Rhodes et al. [RhoR90] in the TEXT tokamak, Langmuir probes were used to measure the electron density fluctuations during the arrival of the heat pulse at the plasma edge. They found that the level of density fluctuations at the edge remained unchanged over the whole sawtooth period.

The disadvantage of the above reported experiments is that they perform a single localized measurement and the dynamical behaviour in the heat pulse propagation region is not adressed. The advantage of the multichannel reflectometer is that this region can be studied for a single heat pulse generated by a sawtooth collapse.

Results of such an experiment are shown in Fig. 11. In the top trace we have plotted the evolution of the electron temperature at 3.39 m, well inside the inversion radius which was located at 3.68 m. The sawtooth crash happened at t=0 and the maximum of the heat pulse generated by the sawtooth arrived at the edge after 10 ms. The following graphs represent the mean square level of the density fluctuations between 50 kHz and 100 kHz, averaged over 250 μs. For the six channels positioned outside the mixing radius, which is at 3.90 m, we do not see any change in the fluctuation level before and after the sawtooth crash. For the reflectometer channel at 3.85 m, situated between the inversion and mixing radius, a threefold increase in density fluctuations is observed from approximately 2 ms before to 1 ms after the collapse. Such a signal has been reported earlier by Brower et al. [BroP87] from a FIR scattering experiment. They observed such an increase in the density fluctuations during the sawtooth crash for a scattering volume positioned just outside the inversion radius. The oscillatory behaviour of the high frequency density fluctuation power as presented in Fig. 11 could be related to the observed m=1 pre- and postcursors but more clear experimental evidence must be gathered to support this.

The results of the reflectometer measurements outside the mixing radius do not

support the model in which χ^{eff} is enhanced directly after the sawtooth crash, because no increase of the turbulence level has been found immidiately after the sawtooth crash. However, it must be remarked that caution is needed when correlating the fluctuation level to a transport coefficient. In particular a change of the radial correlation length can affect the transport coefficient even if the fluctuation level remains constant.

5.3 L-mode to H-mode transition

In the H-mode state of plasmas a transport barrier is formed at the plasma edge resulting in a much better confinement giving rise to steep electron density gradients at the edge as shown in Fig. 12. We have obtained density fluctuation spectra before and after the L-mode to H-mode transition for critical density layers of $n_e = 0.73\ 10^{19}$ and $n_e = 3.14\ 10^{19}\ m^{-3}$. The first layer is situated at the very edge whereas the second layer is 20 cm to 50 cm inside the plasma. The spectra are shown in Fig. 13. In the upper part (the fluctuations spectra at $3.14\ 10^{19}\ m^{-3}$) we see that, except from the appearance of some MHD modes up to 30 kHz, there are no significant changes in the L-mode and H-mode spectra. In the lower part (the fluctuations spectra at $0.73\ 10^{19}\ m^{-3}$) a significant drop of at least a factor five is observed for almost all frequencies when the plasma goes from L-mode to H-mode. From these observations it is concluded that the radial displacement fluctuations, $\tilde{x}$, as observed with the reflectometer are reduced significantly at the edge. This does not imply directly that the density fluctuations, $\tilde{n}$, are reduced as well because the edge gradient increases by at least a factor of three, from $\nabla n_e = 1.1\ 10^{20}\ m^{-4}$ in the L-mode phase to $\nabla n_e \geq 3.3\ 10^{20}\ m^{-4}$ in the H-mode phase (see Fig. 12).

6. Discussion and Conclusions

In this paper we have studied electron density fluctuations using the homodyne detector system of the JET multichannel reflectometer. First, we have investigated the behaviour of the homodyne detectors to amplitude and phase fluctuations. It was found that due to the highly non-linear response, spurious signals are generated at higher harmonics of the fluctuations. The phase fluctuations are mainly caused by rapid movements of the critical density layers around their equilibrium positions whereas the amplitude fluctuations are caused by the reflecting properties of the layers. In the homodyne

detection system these two signals are mixed, which makes it difficult to obtain unambiguous information on the size of the radial displacements of the fluctuations. However, for MHD modes which are also detected with pick-up coils we could often estimate an upper limit of 0.5 cm for those displacements.

In order to obtain signals which can be interpreted without the difficulties of the non-linear phase response and the ambiguities caused by the mixture of phase and amplitude fluctuations, the homodyne detectors should be replaced by fast phase detectors. The phase signal alone contains information on the size of the displacements, $\tilde{x}$, of the of the density fluctuation and the direction of the movement can be obtained in this way as well.

From a further investigation of the observed discrete MHD modes we have learned that in most cases these modes are localized in small regions of the plasma, often coinciding with rational q-surfaces.

It was somewhat surprising to find that in high-β discharges the fishbone activity was not solely localized near the q=1 surface but it had much stronger components at the plasma edge. In low-β discharges the fishbone activity was found to be located at the q=1 surface.

In all density fluctuation spectra, we have observed a background of broadband density fluctuations. We have studied the high frequency (50 kHz to 100 kHz) behaviour of this background during and after a sawtooth crash. In the heat pulse propagation region, we did not find any evidence for an increase of the level of density fluctuations after the sawtooth crash. Inside the mixing radius and from about 2 ms before to 1 ms after the time of the sawtooth crash we do observe an enhancement of the density fluctuations. Such an enhancement was reported earlier by Brower et al. [BroP87] and is related to the crash itself rather than to the heat pulse.

The broadband background of density fluctuations was also subject of our study where the L-mode to H-mode was involved. It was found that in the H-mode the radial fluctuations, $\tilde{x}$, were reduced by more than a factor 5 in the edge, in contrast the bulk plasma, where no change was observed. The reduction of $\tilde{n}$ is much less pronounced, less than a factor of two, because of the increased edge density gradient in the H-mode. In fact the reflectometer data does not exclude the possibility that $\tilde{n}$ remains unchanged and that the reduction of $\tilde{x}$ is entirely due to the increase of ∇n. In view of the large reduction of transport in the edge layer, it might be speculated that $\tilde{x}$ is the parameter

relevant for transport rather than $\tilde{n}$.

Acknowledgements

The authors would like to thank Drs S. Ali-Arshad, A.E. Costley, H.J. de Blank, G.T.A. Huysmans, A.C. Maas, M.F. Nave, F.C. Schüller, P. Smeulders and P.E. Stott for useful discussions. This work was performed under the Euratom-FOM association agreement with the financial support from NWO and Euratom.

references

[Liew85] P.C. Liewer, Nucl. Fusion, **25**, 331 (1985).

[RhoR90] T.L. Rhodes, Ch.P. Ritz and H. Lin, Phys. Rev. Lett. **65**, 583 (1990).

[SchC88] P.M. Schoch, A. Carnevali, K.A. Conner, T.P. Crowley, J.C. Forster, R.L.Hickok, J.F. Lewis, J.G. Schatz, G.A. Hallock, Rev. Sci. Instrum. **59**, 1646 (1988).

[BroP87] D.L. Brower, W.A. Peebles, S.K. Kim and N.C. Luhmann,
Proc. of the fourteenth European Conference on Controlled Fusion and Plasma Heating, Madrid, 1314 (1987).

[IAEA92] IAEA Technical Committee Meeting Microwave Reflectometry for Fusion Plasma Diagnostics. IAEA, Vienna, Austria (1992).

[HolR92b] E. Holzhauer and T.L.Rhodes, IAEA Technical Committee Meeting Microwave Reflectometry for Fusion Plasma Diagnostics. IAEA, Vienna, Austria 97 (1992).

[Crip92] P.J. Cripwell, Extraordinary Mode Reflectometry at JET. Ph.D thesis, University of London (1992), IAEA Technical Committee Meeting Microwave Reflectometry for Fusion Plasma Diagnostics. IAEA, Vienna, Austria 79 (1992) and JET report JET-P(92)55 25 (1992).

[Hutc92] I.H. Hutchinson, IAEA Technical Committee Meeting Microwave Reflectometry for Fusion Plasma Diagnostics. IAEA, Vienna, Austria 79 (1992).

[HolR92a] E. Holzhauer and T.L.Rhodes, IAEA Technical Committee Meeting Microwave Reflectometry for Fusion Plasma Diagnostics. IAEA, Vienna, Austria 89 (1992).

[HugP86] C.A.J. Hugenholtz and A.J. Putter, Workshop on Basic and Advanced Diagnostic Techniques for Fusion Plasmas, Varenna, EUR 10797 EN Vol **II** 469 (1986).

[PreC86] R. Prentice, A.E. Costley, J.A. Fessey and A.E. Hubbard,
Workshop on Basic and Advanced Diagnostic Techniques for Fusion Plasmas, Varenna, EUR 10797 EN Vol **II** 451 (1986).

[SipK92] A.C.C. Sips, G.J. Kramer, M. Beurskens, A.E. Costley and R. Prentice, IAEA Technical Committee Meeting Microwave Reflectometry for Fusion Plasma Diagnostics. IAEA, Vienna, Austria 11 (1992) and JET report JET-P(92)55 1 (1992).

[HogR91] D. Hogeweij, J. O'Rourke and A.C.C. Sips, Plasma Phys. and Contr. Fusion, **33** 189 1991.

[ColC92] A. Colton and P.J. Cripwell, IAEA Technical Committee Meeting Microwave Reflectometry for Fusion Plasma Diagnostics. IAEA, Vienna, Austria 157 (1992) and JET report JET-P(92)55 55 (1992).

[KraS92] G.J. Kramer, A.C.C. Sips and A.E. Costley, IAEA Technical Committee Meeting Microwave Reflectometry for Fusion Plasma Diagnostics. IAEA, Vienna, Austria 143 (1992) and JET report JET-P(92)55 39 (1992).

[Sips91] A.C.C. Sips, Reflectometry and Transport in Thermonuclear Plasmas in the Joint European Torus, Ph.D thesis, Technical University Eindhoven 47 (1991).

[Huge90] C.A.J. Hugenholtz, Microwave Interferometer and Reflectometer Techniques for Thermonuclear Plasmas Ph.D thesis, Technical University Eindhoven 38 (1991).

[CriC92] P.J. Cripwell, A.E. Costley and T. Fukuda, IAEA Technical Committee Meeting Microwave Reflectometry for Fusion Plasma Diagnostics. IAEA, Vienna, Austria 168 (1992). and JET report JET-P(92)55 69 (1992).

[NavC90] M.F.F. Nave, D. Campbell, E. Joffrin, F.B. Marcus, G. Sadler, P. Smeulders and K. Thomson, Nucl. Fusion **31** 697 (1991) and JET report JET-P(90)32 69 (1990).

[TubL87] B.J.D. Tubbing, N.J. Lopes Cardozo and M.J. van der Wiel, Nucl. Fusion **27** 1843 (1987).

[FreM90] E.D. Fredrickson, K. McGuire, A. Cavallo, R. Budny, A. Janos, D. Monticello, Y. Nagayama, W. Park, G. Taylor and M.C. Zarnstroff,
Phys. Rev. Lett. **65**, 2869 (1990).

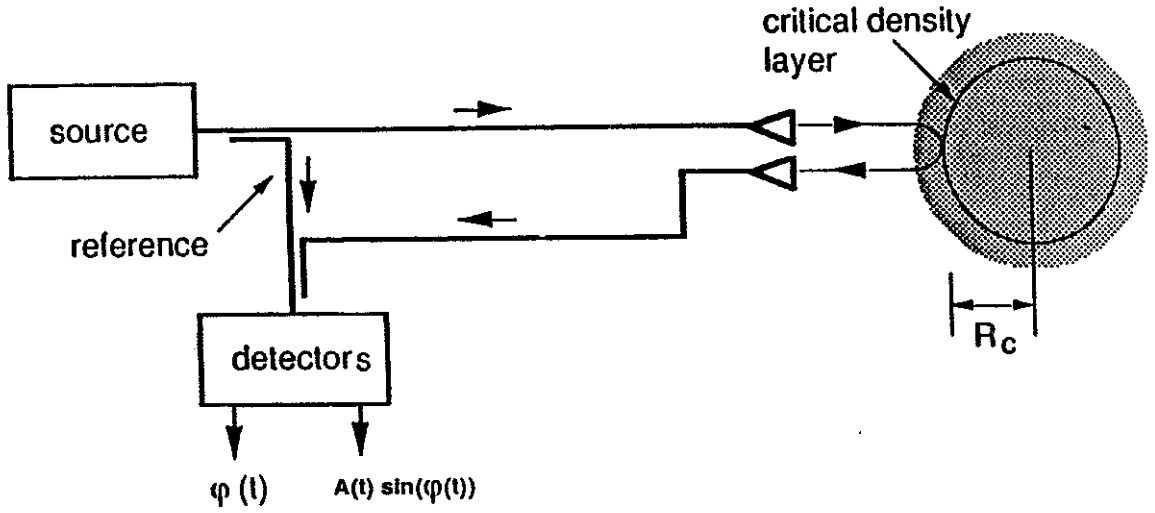

Fig. 1 The basic set-up of one channel of the JET reflectometer. The microwaves which are generated in the source are transported to the plasma where they are reflected at the critical density layer. In the detector system the reflected signal is combined with the reference signal to obtain the (narrow band) phase signal, $\phi(t)$, for electron density profile measurements and the (broad band) homodyne signal, $A(t)\sin(\phi(t))$, for electron density fluctuation measurements.

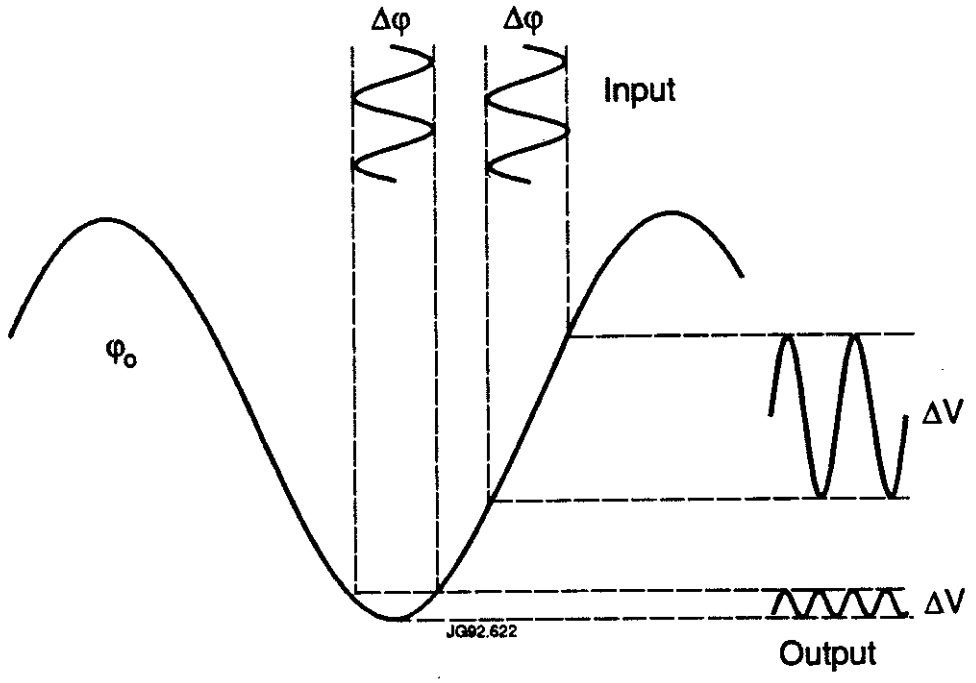

Fig. 2 The response of the homodyne detector system to phase fluctuations, indicated here as $\Delta\phi$. Depending on the equilibrium phase, ϕ_0, one gets different non-linear responses. Indicated in this graph are two extremes, a nearly linear response (upper trace ΔV in the output) and a case where frequency doubling takes place (lower trace ΔV in the output).

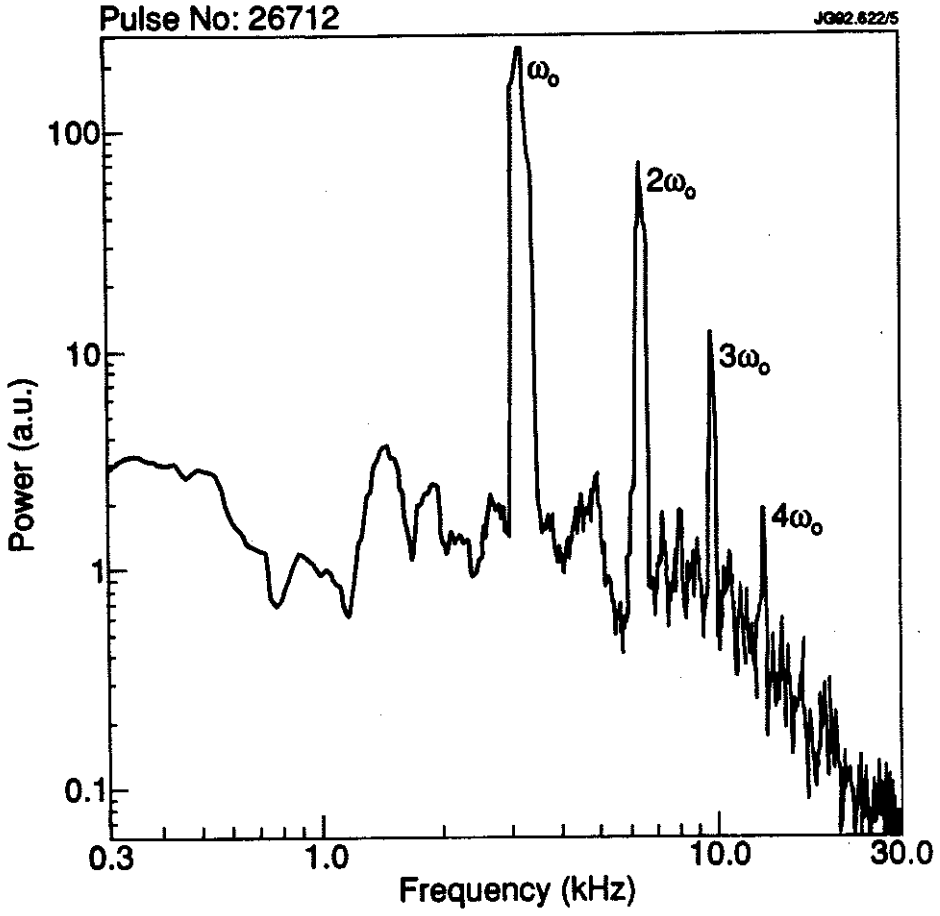

Fig. 3 A density fluctuation spectrum in which harmonics of the discrete mode are observed. They are generated by the frequency doubling properties of the homodyne detection system. In Fig. 4a this signal is shown as a function of time.

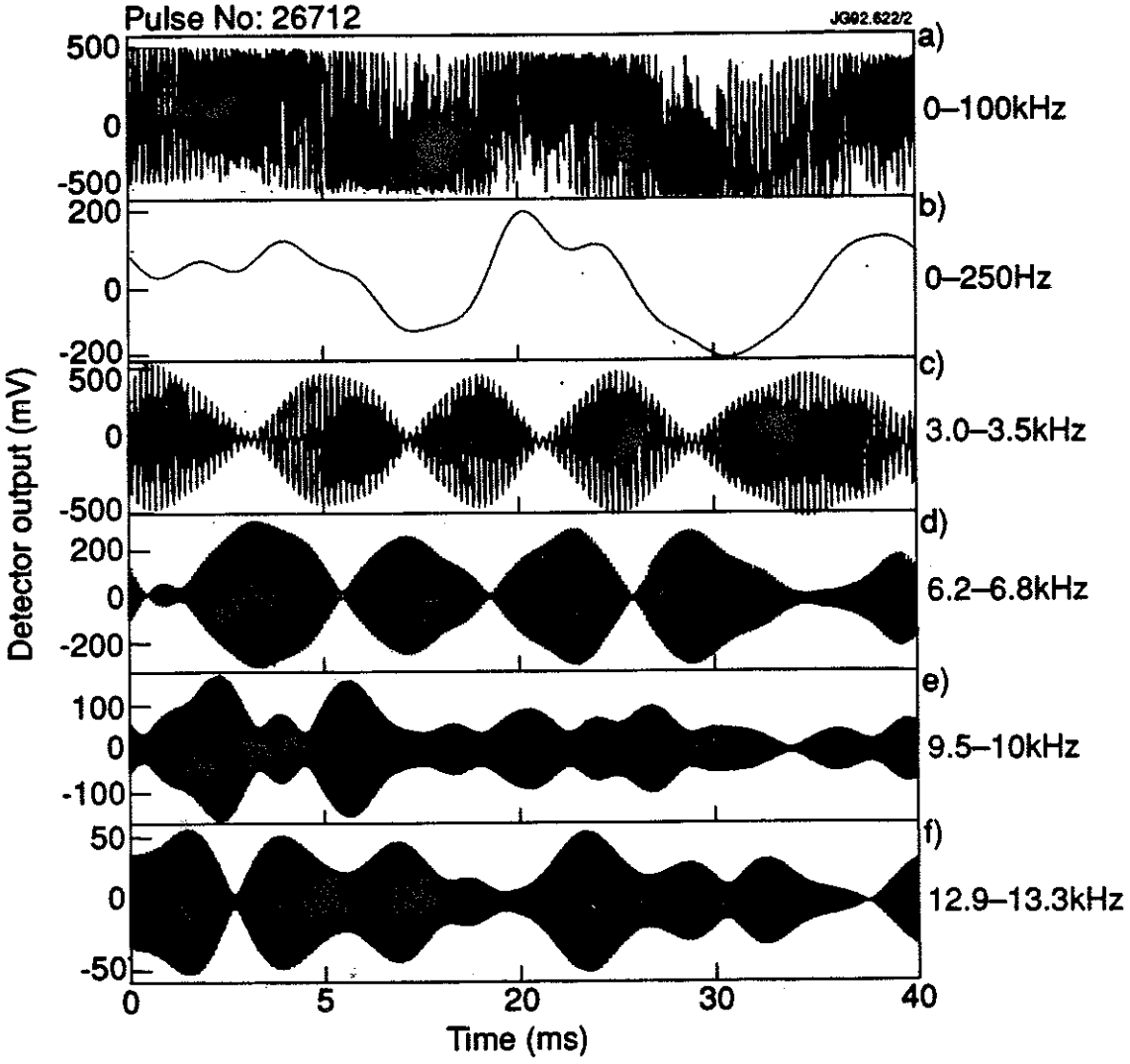

Fig. 4 The total signal (trace a) and the band-pass filtered signals of the fundamental frequency (trace c, 3.2 kHz, ω_0 in Fig. 3) and its harmonics, (traces d, e and f). In trace b the slow frequency components are shown.

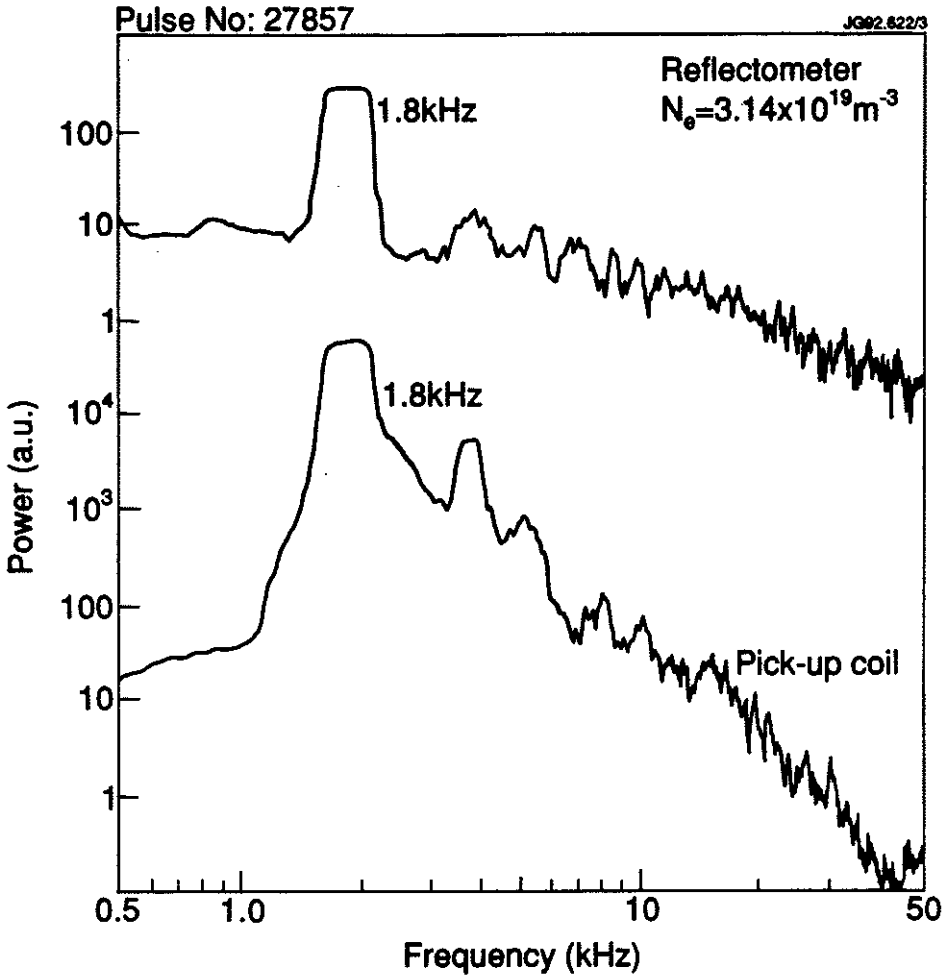

Fig. 5 A density fluctuation spectrum taken with the reflectometer at a critical density layer of 3.14 10^{19} m^{-3} (upper trace) compared to a spectrum obtained from a magnetic pick-up coil (lower trace). In both spectra the 1.8 kHz frequency of the fishbone is clearly visible. The time traces of these signals are shown in Fig. 6.

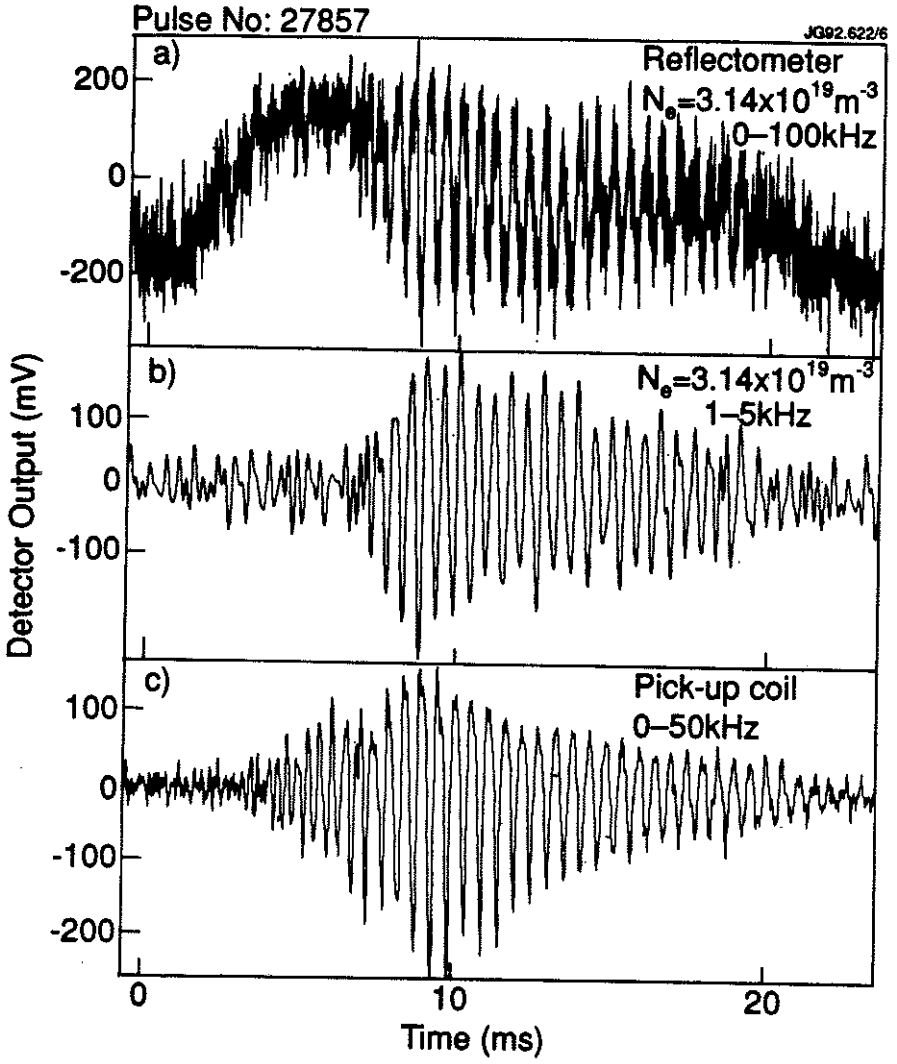

Fig. 6 Fishbone activity as observed with the reflectometer (upper panel) and with a magnetic pick-up coil (lower panel). In the middle panel we have applied a digital bandpass filter (1 kHz to 5 kHz) to the reflectometer signal in order to show the (low frequency) correlation with the magnetic signal more clearly. Note the suppression of the fishbone signal between 4 and 8 miliseconds due to the nonlinear behaviour of the homodyne detection system.

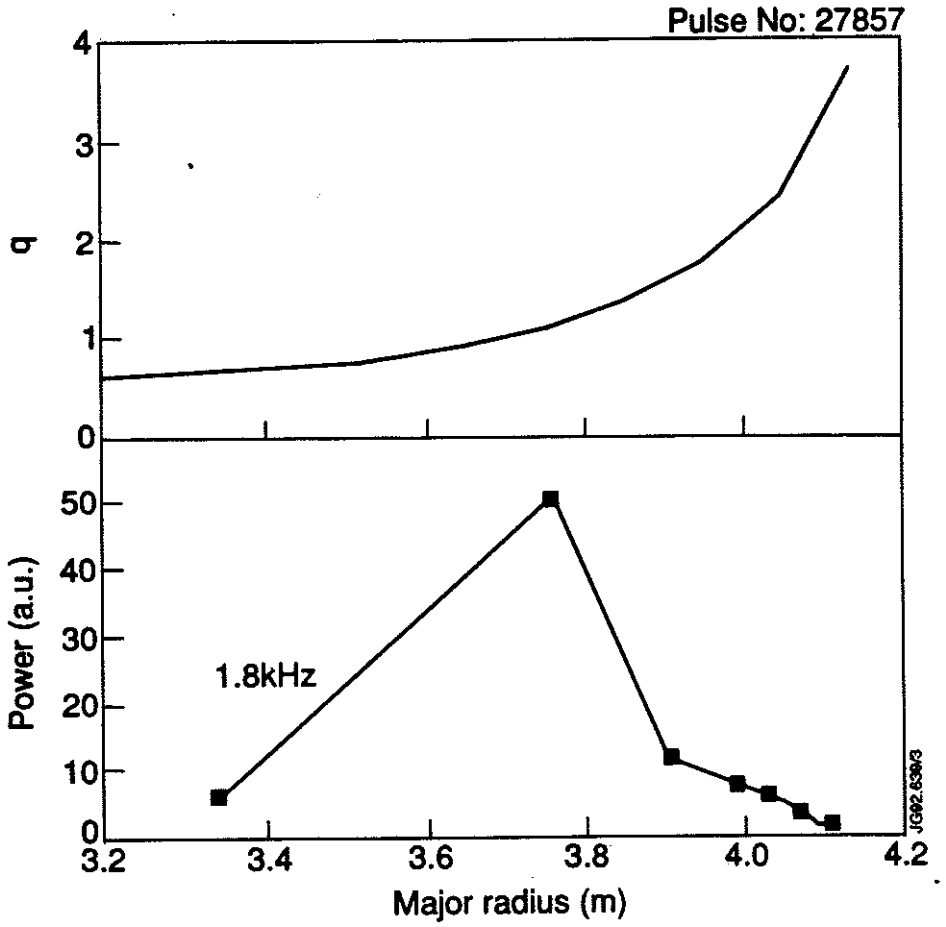

Fig. 7 The radial extent of the fishbone shown in Fig. 6 as determined from the eight reflectometer channels, indicated with the squares in the lower panel, which were reflected inside the plasma. The ratio of the power of at the MHD mode over the background power is plotted (see also sec. 2) as a function of the major radius. The line is drawn to guide the eye. In the upper panel the q-profile is shown.

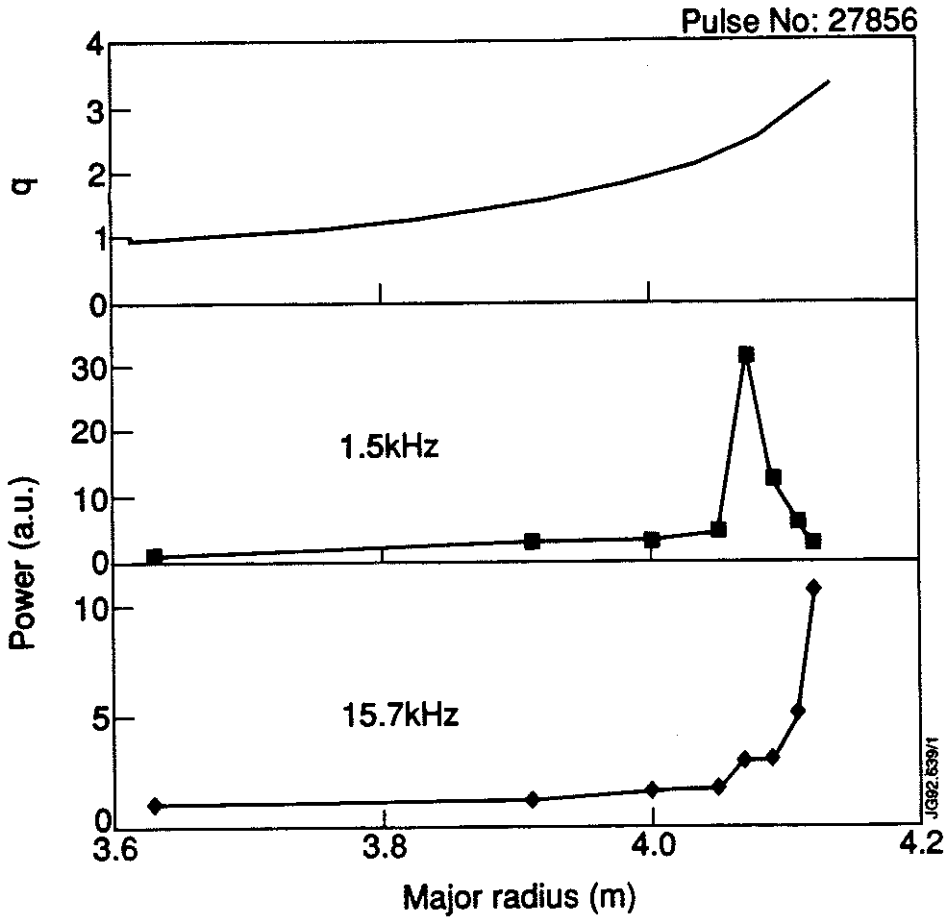

Fig. 8 The radial extent of two other MHD modes as observed in a similar discharge in which the fishbone of Fig. 7 observed. The 1.5 kHz mode seems to coincide with the q=2.5 surface whereas the 15.7 kHz mode is located at the plasma edge. The position of the eight reflectometer channel which were reflected inside the plasma are indicated with the squares and the lines are drawn to guide the eye. The ratio of the power of at the MHD mode over the background power is plotted (see also sec. 2) as a function of the major radius. In the upper panel the q-profile is shown.

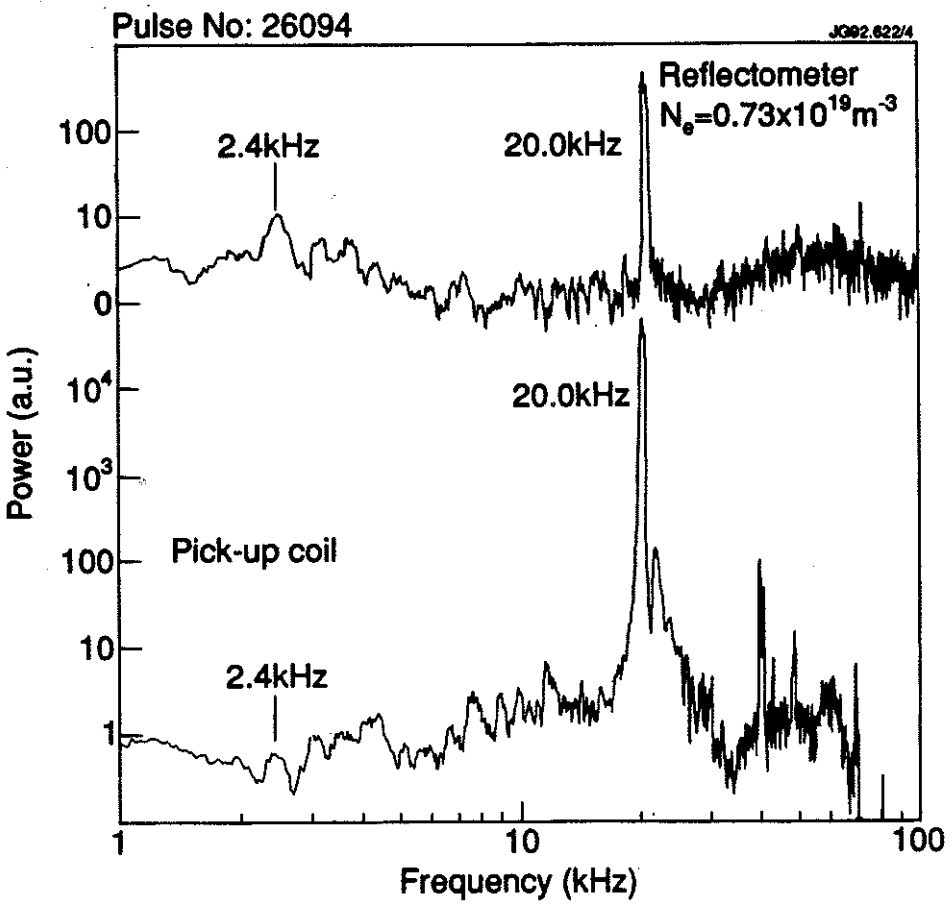

Fig. 9 A density fluctuation spectrum taken with the reflectometer at a critical density layer of 0.73 10^{19} m^{-3} (upper trace) compared to a spectrum obtained from a magnetic pick-up coil (lower trace). In both spectra the 20 kHz frequency of the fishbone is very clearly visible. The 2.4 kHz mode is indicated as well.

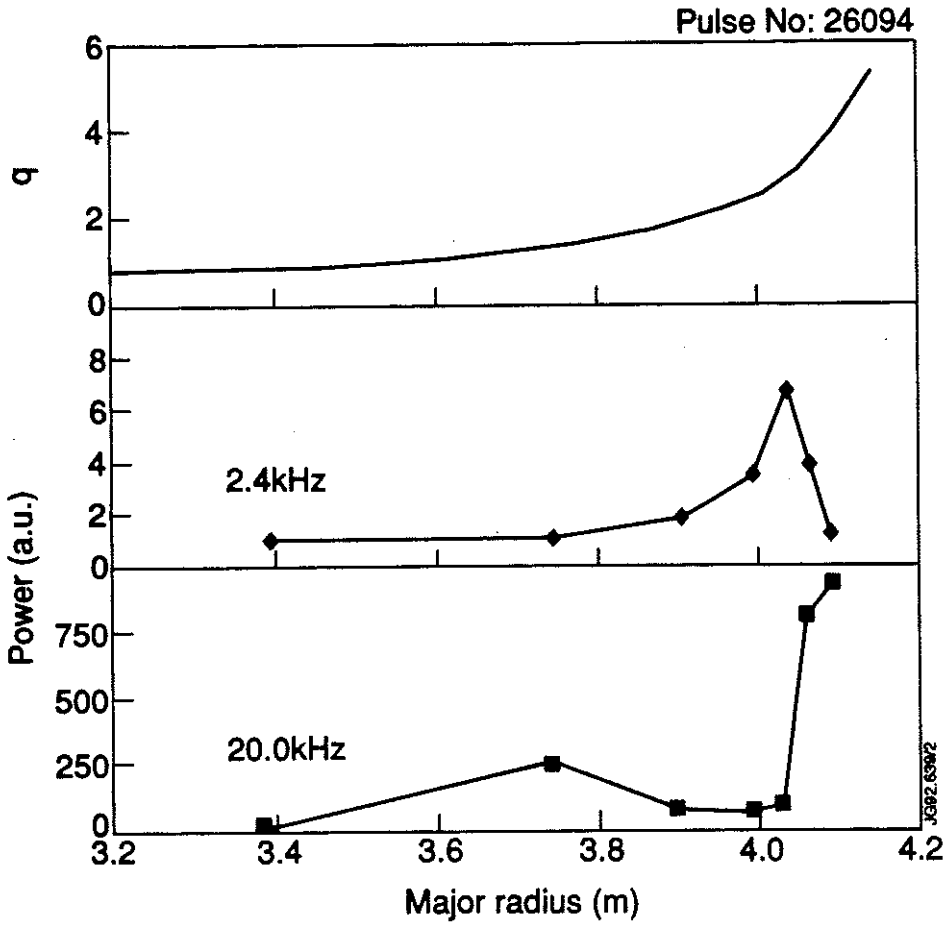

Fig. 10 The radial extent of two MHD modes as observed in a high-β discharge. The mode at 20 kHz is identified as a fishbone. In contrast to the fishbone activity shown in Fig. 7, this fishbone is not only located at the q=1 surface but it has also a strong component at the plasma edge. The 2.4 kHz mode has its maximum at the q=3 surface and a decrease towards the edge. From this we conclude that the applied normalization is not the cause of the edge component. The ratio of the power of at the MHD mode over the background power is plotted (see also sec. 2) as a function of the major radius. In the upper panel the q-profile is shown.

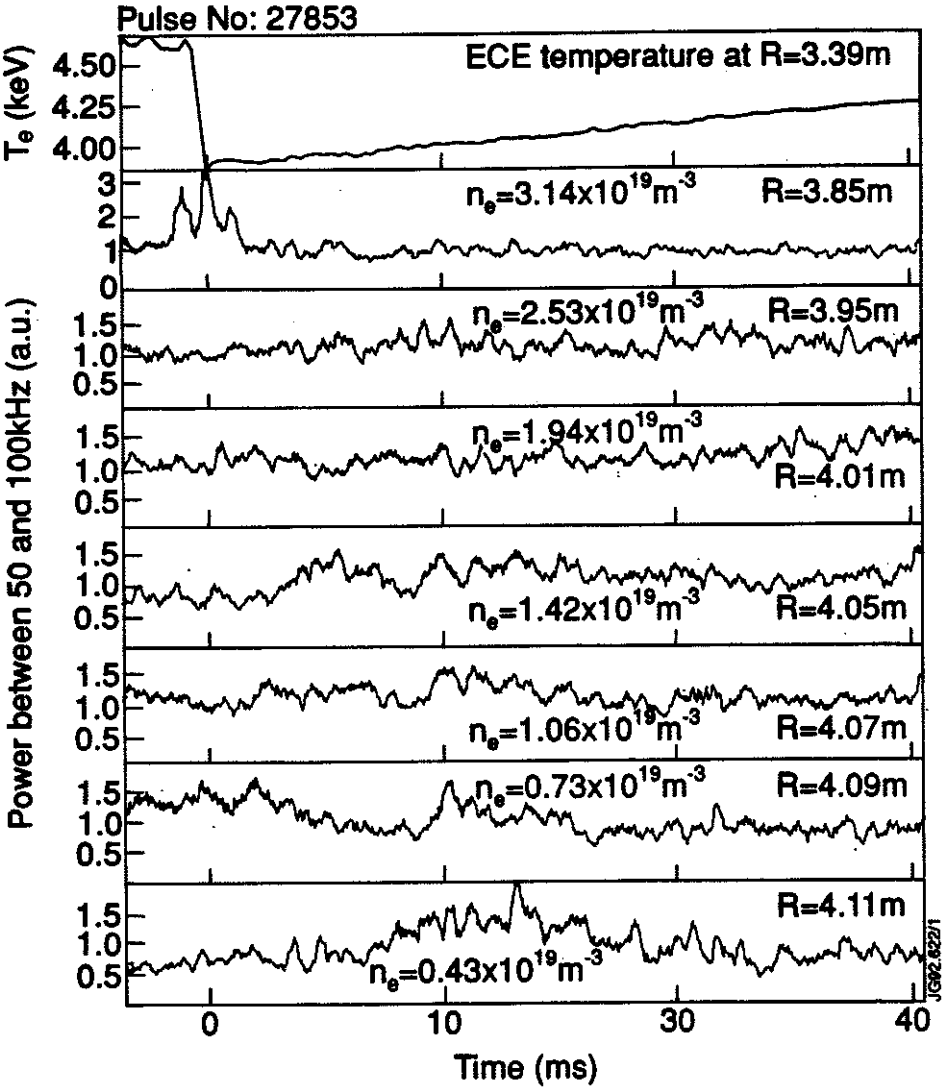

Fig. 11 The behaviour of the density fluctuation power between 50 kHz and 100 kHz. The upper trace is the electron temperature at a major radius of 3.39 m showing the time of the sawtooth crash. The second trace, at 3.85 m is a reflectometer channel positioned between the inversion radius (3.68 m) and the mixing radius (3.90 m). In this channel we observe a threefold increase in the high frequency fluctuation level but only around the time of the sawtooth crash. The other channels (the traces between 3.95 and 4.11 m) which are all situated in the heat pulse propagation region do not show a measurable change in their fluctuation levels.

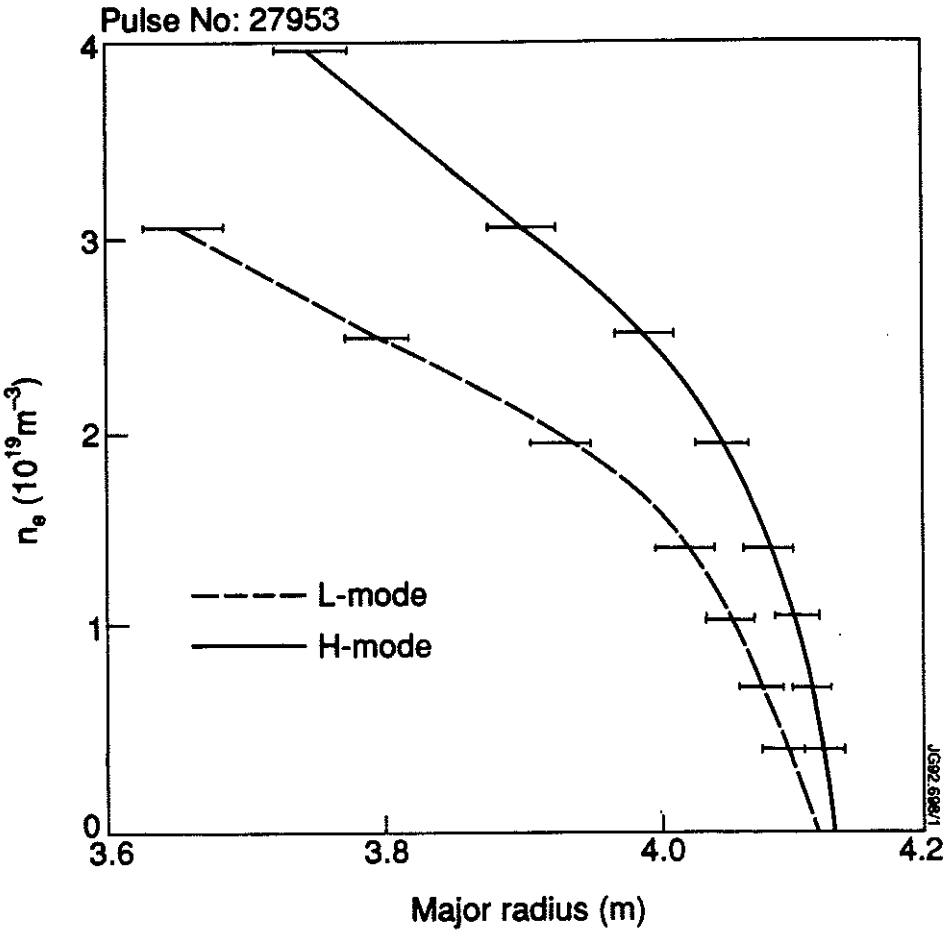

Fig. 12 The electron density profiles as obtained from the reflectometer in the L-mode (dashed curve) and H-mode (full curve) at the times when the spectra as shown in fig. 13 are obtained.

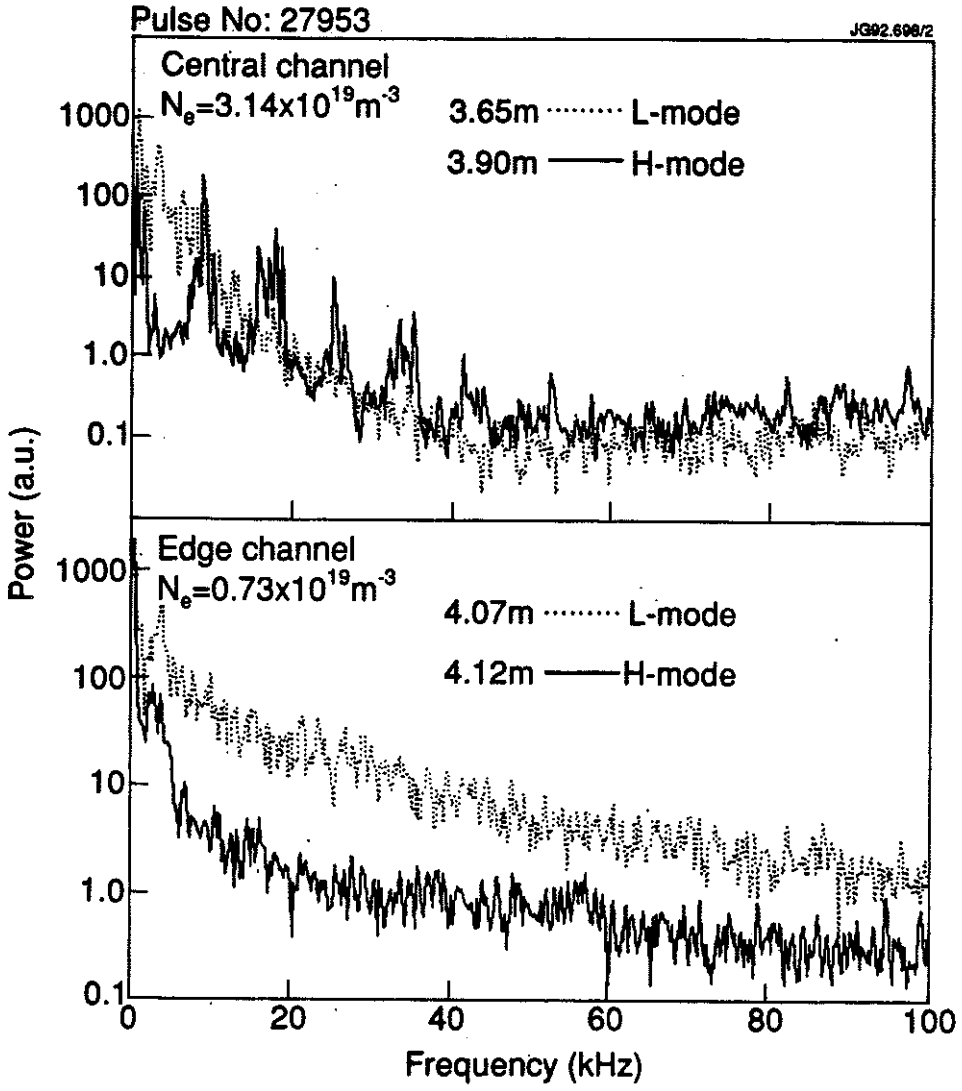

Fig. 13 Density fluctuation spectra as obtained during the L-mode and H-mode phases for a NBI heated discharge. In the top panel a channel which is probing the bulk plasma is shown. No drop in the fluctuation level is found after the L-mode to H-mode transition. In the bottom panel a channel which is probing the plasma edge is shown. A significant drop in the fluctuation level is observed. Note the linear scale for the frequency axis.

channel	frequency (GHz)	crit. dens. ($10^{19}m^{-3}$)
1	18.6	0.43
2	24.3	0.73
3	29.3	1.06
4	33.8	1.42
5	39.5	1.94
6	45.2	2.53
7	50.3	3.14
8	57.1	4.05
9	64.2	5.11
10	69.5	6.00
11	75.1	7.00
12	80.2	7.98

Table 1 The twelve frequencies which are used in the JET reflectometer, and the corresponding critical densities.

pulse	26094 H	27853 L	27856 L	27857 L	27953 L	27953 H
I_{pla}	3.1 MA	7.0 MA	7.0 MA	7.0 MA	3.0 MA	
B_T	2.8 T	3.4 T	3.4 T	3.4 T	2.8 T	
β_{tor}	22 10^{-3}	7.0 10^{-3}	7.1 10^{-3}	9.6 10^{-3}	2.8 10^{-3}	8.4 10^{-3}
HEATING						
ohmic	1.0 MW	5.8 MW	5.9 MW	5.5 MW	1.5 MW	
NBI	14.0 MW	—	—	7.0 MW	2.0 MW	11.0 MW
RF	—	5.5 MW	5.0 MW	5.5 MW	—	

Table 2 The main plasma parameters for the dischargers which were used in this in this paper.

Appendix I

THE JET TEAM

JET Joint Undertaking, Abingdon, Oxon, OX14 3EA, U.K.

J.M. Adams[1], B. Alper, H. Altmann, A. Andersen[14], P. Andrew, S.Ali-Arshad, W. Bailey, B. Balet, P. Barabaschi, Y. Baranov, P. Barker, R. Barnsley[2], M. Baronian, D.V. Bartlett, A.C. Bell, G. Benali, P. Bertoldi, E. Bertolini, V. Bhatnagar, A.J. Bickley, D. Bond, T. Bonicelli, S.J. Booth, G. Bosia, M. Botman, D. Boucher, P. Boucquey, M. Brandon, P. Breger, H. Brelen, W.J. Brewerton, H. Brinkschulte, T. Brown, M. Brusati, T. Budd, M. Bures, P. Burton, T. Businaro, P. Butcher, H. Buttgereit, C. Caldwell-Nichols, D.J. Campbell, D. Campling, P. Card, G. Celentano, C.D. Challis, A.V.Chankin[23], A. Cherubini, D. Chiron, J. Christiansen, P. Chuilon, R. Claesen, S. Clement, E. Clipsham, J.P. Coad, I.H. Coffey[24], A. Colton, M. Comiskey[4], S. Conroy, M. Cooke, S. Cooper, J.G. Cordey, W. Core, G. Corrigan, S. Corti, A.E. Costley, G. Cottrell, M. Cox[7], P. Crawley, O. Da Costa, N. Davies, S.J. Davies[7], H. de Blank, H. de Esch, L. de Kock, E. Deksnis, N. Deliyanakus, G.B. Denne-Hinnov, G. Deschamps, W.J. Dickson[19], K.J. Dietz, A. Dines, S.L. Dmitrenko, M. Dmitrieva[25], J. Dobbing, N. Dolgetta, S.E. Dorling, P.G. Doyle, D.F. Düchs, H. Duquenoy, A. Edwards, J. Ehrenberg, A. Ekedahl, T. Elevant[11], S.K. Erents[7], L.G. Eriksson, H. Fajemirokun[12], H. Falter, J. Freiling[15], C. Froger, P. Froissard, K. Fullard, M. Gadeberg, A. Galetsas, L. Galbiati, D. Gambier, M. Garribba, P. Gaze, R. Giannella, A. Gibson, R.D. Gill, A. Girard, A. Gondhalekar, D. Goodall[7], C. Gormezano, N.A. Gottardi, C. Gowers, B.J. Green, R. Haange, A. Haigh, C.J. Hancock, P.J. Harbour, N.C. Hawkes[7], N.P. Hawkes[1], P. Haynes[7], J.L. Hemmerich, T. Hender[7], J. Hoekzema, L. Horton, J. How, P.J. Howarth[5], M. Huart, T.P. Hughes[4], M. Huguet, F. Hurd, K. Ida[18], B. Ingram, M. Irving, J. Jacquinot, H. Jaeckel, J.F. Jaeger, G. Janeschitz, Z. Jankowicz[22], O.N. Jarvis, F. Jensen, E.M. Jones, L.P.D.F. Jones, T.T.C. Jones, J-F. Junger, F. Junique, A. Kaye, B.E. Keen, M. Keilhacker, W. Kerner, N.J. Kidd, R. Konig, A. Konstantellos, P. Kupschus, R. Lässer, J.R. Last, B. Laundy, L. Lauro-Taroni, K. Lawson[7], M. Lennholm, J.Lingertat[13], R.N. Litunovski, A. Loarte, R. Lobel, P. Lomas, M. Loughlin, C. Lowry, A.C. Maas[15], B. Macklin, C.F. Maggi[16], G. Magyar, V. Marchese, F. Marcus, J. Mart, D. Martin, E. Martin, R. Martin-Solis[8], P. Massmann, G. Matthews, H. McBryan, G. McCracken[7], P. Meriguet, P. Miele, S.F. Mills, P. Millward, E. Minardi[16], R. Mohanti[17], P.L. Mondino, A. Montvai[3], P. Morgan, H. Morsi, G. Murphy, F. Nave[27], S. Neudatchin[23], G. Newbert, M. Newman, P. Nielsen, P. Noll, W. Obert, D. O'Brien, J. O'Rourke, R. Ostrom, M. Ottaviani, S. Papastergiou, D. Pasini, B. Patel, A. Peacock, N. Peacock[7], R.J.M. Pearce, D. Pearson[12], J.F. Peng[26], R. Pepe de Silva, G. Perinic, C. Perry, M.A. Pick, J. Plancoulaine, J-P. Poffé, R. Pohlchen, F. Porcelli, L. Porte[19], R. Prentice, S. Puppin, S. Putvinskii[23], G. Radford[9], T. Raimondi, M.C. Ramos de Andrade, M. Rapisarda[29], P-H. Rebut, R. Reichle, S. Richards, E. Righi, F. Rimini, A. Rolfe, R.T. Ross, L. Rossi, R. Russ, H.C. Sack, G. Sadler, G. Saibene, J.L. Salanave, G. Sanazzaro, A. Santagiustina, R. Sartori, C. Sborchia, P. Schild, M. Schmid, G. Schmidt[6], H. Schroepf, B. Schunke, S.M. Scott, A. Sibley, R. Simonini, A.C.C. Sips, P. Smeulders, R. Smith, M. Stamp, P. Stangeby[20], D.F. Start, C.A. Steed, D. Stork, P.E. Stott, P. Stubberfield, D. Summers, H. Summers[19], L. Svensson, J.A. Tagle[21], A. Tanga, A. Taroni, C. Terella, A. Tesini, P.R. Thomas, E. Thompson, K. Thomsen, P. Trevalion, B. Tubbing, F. Tibone, H. van der Beken, G. Vlases, M. von Hellermann, T. Wade, C. Walker, D. Ward, M.L. Watkins, M.J. Watson, S. Weber[10], J. Wesson, T.J. Wijnands, J. Wilks, D. Wilson, T. Winkel, R. Wolf, D. Wong, C. Woodward, M. Wykes, I.D. Young, L. Zannelli, A. Zolfaghari[28], G. Zullo, W. Zwingmann.

PERMANENT ADDRESSES

1. UKAEA, Harwell, Didcot, Oxon, UK.
2. University of Leicester, Leicester, UK.
3. Central Research Institute for Physics, Budapest, Hungary.
4. University of Essex, Colchester, UK.
5. University of Birmingham, Birmingham, UK.
6. Princeton Plasma Physics Laboratory, New Jersey, USA.
7. UKAEA Culham Laboratory, Abingdon, Oxon, UK.
8. Universidad Complutense de Madrid, Spain.
9. Institute of Mathematics, University of Oxford, UK.
10. Freien Universität, Berlin, F.R.G.
11. Royal Institute of Technology, Stockholm, Sweden.
12. Imperial College, University of London, UK.
13. Max Planck Institut für Plasmaphysik, Garching, FRG.
14. Risø National Laboratory, Denmark.
15. FOM Instituut voor Plasmafysica, Nieuwegein, The Netherlands.
16. Dipartimento di Fisica, University of Milan, Milano, Italy.
17. North Carolina State University, Raleigh, NC, USA
18. National Institute for Fusion Science, Nagoya, Japan.
19. University of Strathclyde, 107 Rottenrow, Glasgow, UK.
20. Institute for Aerospace Studies, University of Toronto, Ontario, Canada.
21. CIEMAT, Madrid, Spain.
22. Institute for Nuclear Studies, Otwock-Swierk, Poland.
23. Kurchatov Institute of Atomic Energy, Moscow, USSR
24. Queens University, Belfast, UK.
25. Keldysh Institute of Applied Mathematics, Moscow, USSR.
26. Institute of Plasma Physics, Academica Sinica, Hefei, P. R. China.
27. LNETI, Savacem, Portugal.
28. Plasma Fusion Center, M.I.T., Boston, USA.
29. ENEA, Frascati, Italy.

At 1st July, 1992